Journal of Catalysis 272 (2010) 195–203

Contents lists available at ScienceDirect

Journal of Catalysis

journal homepage: www.elsevier.com/locate/jcat

Comparative atomic-scale analysis of promotional effects by late 3d-transition metals in MoS_2 hydrotreating catalysts

Jakob Kibsgaard [a,1], Anders Tuxen [a], Kim G. Knudsen [b], Michael Brorson [b], Henrik Topsøe [b], Erik Lægsgaard [a], Jeppe V. Lauritsen [a,*], Flemming Besenbacher [a]

[a] Interdisciplinary Nanoscience Center (iNANO), Department of Physics and Astronomy, Aarhus University, DK-8000 Århus C, Denmark
[b] Haldor Topsøe A/S, Nymøllevej 55, DK-2800 Lyngby, Denmark

ARTICLE INFO

Article history:
Received 1 February 2010
Revised 25 March 2010
Accepted 26 March 2010

Keywords:
Catalysis
Hydrotreating
Hydrodesulfurization
Promoters
Co–Mo–S
MoS_2
Activity measurements
Scanning tunneling microscopy
Nanoclusters
Nanoparticles

ABSTRACT

The promotion of the activity of MoS_2-based hydrotreating catalysts by various first-row transition metals exhibits a typical variation referred to as a volcano plot. Co and Ni are seen to substantially promote the catalytic activity of MoS_2, whereas the neighboring first-row metals promote reactivity to a much lesser extent, or not at all. In order to provide a better atomistic understanding of the catalytic synergies, we perform here a comparative scanning tunneling microscopy (STM) analysis of the atomic-scale structure and morphology of MoS_2 nanoclusters doped with the first-row transition metals: Fe, Co, Ni, and Cu. We reveal that addition of all four dopant metals results in the formation of mixed-metal "Co–Mo–S"-type structures shaped as single-layer hexagonally truncated triangular MoS_2-like nanoclusters. The modification of the preferred nanocluster equilibrium morphology is explained as a direct consequence of a favored substitution of dopant metal atoms into the S-edges of MoS_2. The degree of truncation and the edge dispersion are, however, found to depend greatly on the type of dopant atom since the relative length of the dopant-stabilized edges decreases with the number of valence shell electrons of the dopant transition metal. A comparison of the observed atomic structure and morphology with the hydrotreating activity measured for industrial-style prepared Me–Mo–S catalysts (Me = Fe, Co, Ni, and Cu) supported on carbon reveals that two parameters are relevant to describe the promotional behavior: (i) a geometric parameter, which relates to the relative number of promoted and unpromoted sites in the Me–Mo–S nanoclusters, and (ii) a more conventional parameter relating to bonding and adsorption strength, i.e., describing the intrinsic activity of the particular Me-doped S-edge.

1. Introduction

The hydrotreating catalyst plays a key role in pollution reduction as it in refinery processes catalyzes the removal of sulfur from oil of fossil origin before this oil is used as transportation fuel. The catalysts used for this purpose are based on transition metal sulfide mixtures (Co/Ni and MoS_2) typically dispersed on a high surface area aluminum oxide carrier [1,2]. Research efforts in the field of hydrotreating catalysis have recently increased significantly due to the urgent requirements of ultra-low sulfur contents in diesel transportation fuels and the need to process increasingly heavier crude oils. However, the traditional, empirically discovered mixed metal sulfides based on Co/Ni and MoS_2 (or WS_2) remain the catalysts of choice. MoS_2 itself is not a particularly active monometallic transition metal sulfide [2,3], but Mo is relatively inexpensive and a great number of studies have shown that two particular first-row transitions metals, Co and Ni, are strong promoters for MoS_2 since both increase the hydrogenation (HYD) and hydrodesulfurization (HDS) activity many fold. In the literature, the widely accepted "Co–Mo–S" model [2,4,5] describes the promoted catalyst in the active state as so-called "Co–Mo–S"-type nanoclusters that are essentially of MoS_2 nature but with promoter atoms (Co or Ni) substituted at the MoS_2 nanocluster edges. The detailed atomic-scale equilibrium structures of the Co–Mo–S and Ni–Mo–S phase have recently been revealed from an interplay between STM [6,7] and density functional theory (DFT) calculations [8–12]. However, the question remains what makes Co and Ni such good promoters? Previous Mössbauer spectroscopic studies have presented evidence of an analogous Fe–Mo–S phase with Fe present in the MoS_2 lattice [2,13–15]. In one study [15], it was found that the addition of Fe decreases the catalytic activity suggesting that the sites associated with the Fe–Mo–S structure are slightly less active than unpromoted MoS_2. However, for carbon-supported Fe–Mo catalysts [14], a slight promotion was observed. In the case of Cu–Mo catalysts, it has not been determined whether

* Corresponding author. Fax: +45 8612 0740.
E-mail address: jvang@inano.au.dk (J.V. Lauritsen).
[1] Present address: Department of Chemical Engineering, Stanford University, Stanford, CA 94305, USA.

0021-9517/$ - see front matter © 2010 Elsevier Inc. All rights reserved.
doi:10.1016/j.jcat.2010.03.018

Cu–Mo–S-type structures form at all, and it has been observed that addition of Cu has no or even a slight inhibiting effect on the HDS activity [2,16].

The traditional models for HDS reactivity have considered sulfur vacancies formed on the nanocluster edges to be the reactive sites, and accordingly the promotional effect has been associated with a modification of the metal–sulfur binding energies at the site where the dopant atoms are located in the Co–Mo–S-type clusters [17–20]. However, for many years, there existed a general lack of insight on the location and coordination of the dopant atoms and, consequently, the nature of the promoting role is not fully understood. Recent STM and DFT studies [21–23] have revealed that creation of sulfur vacancies may not be a necessary requirement for MoS_2 to catalyze HDS and hydrogenation reactions of thiophene (C_4H_4S) due to the presence of so-called brim sites that result from the modified electronic and geometric structure at the edges of the MoS_2 nanoclusters. Such brim sites may be catalytically active without generation of sulfur vacancies. Furthermore, previous STM experiments and theory studies have revealed that Co–Mo–S and Ni–Mo–S clusters in their equilibrium state may expose intrinsic coordinatively undersaturated sites (CUS) [6,7,24].

To provide a better atomistic understanding of the hydrotreating activity and selectivity of MoS_2 nanoclusters promoted with first-row transition metals, we perform here a systematic atomic-scale structural characterization and comparative analysis of bimetallic "Me–Mo–S"-type nanoclusters formed by synthesis of MoS_2 in the presence of various Me promoters (Me = Fe, Co, Ni, and Cu) on an inert Au(1 1 1) model substrate. We present the first atom-resolved images of iron- and copper-doped MoS_2 nanoclusters and show that the Fe–Mo–S and Cu–Mo–S phases have a structure similar to that previously reported of Co–Mo–S and Ni–Mo–S [6,7]. Like Co–Mo–S and Ni–Mo–S, the Cu–Mo–S and Fe–Mo–S nanoclusters do not exhibit a well-defined structure in the crystallographic sense. Rather, all types of Me–Mo–S nanoclusters can be viewed as single-layer, triangular-shaped MoS_2 nanoclusters with truncated corners due to incorporation of Me atoms at specific edge sites. Interestingly, we show that the detailed equilibrium shape of the doped MoS_2 nanoclusters depends on the dopant element in a systematic way, since the proportional length of the Me-stabilized edges decreases when the number of valence shell electrons of the dopant element is increased. This implies that the relative concentration of promoted and unpromoted edge sites in Me–Mo–S nanoclusters depends on the type of promoter atom. From a comparison of the activity measured on high surface area carbon-supported Me–Mo–S catalysts, we show that the promotional effect is controlled by an intrinsic parameter related to the bonding properties of the particular promoted S-edge of Me–Mo–S and a geometric parameter related to the relative concentration of promoted and unpromoted edge sites exposed for a given Me–Mo–S phase. Interestingly, both the intrinsic and the geometric parameter seem to be controlled by the particular Me–S bond strength and an optimum for a high catalytic activity emerges for Co and Ni.

2. Experimental

2.1. Synthesis of hydrotretating model catalyst on Au(1 1 1)

The Me–Mo–S-type nanoclusters were synthesized by physical vapor deposition of metals atoms onto a flat Au(1 1 1) surface followed by sulfidation by pure H_2S(g) at an elevated temperature. As previously demonstrated in detail in the case of Co–Mo–S and Ni–Mo–S [7,25], the use of the herringbone reconstructed Au(1 1 1) surface facilitates the formation of few nanometer-wide Me–Mo–S-type nanoclusters, i.e., mixed metal sulfide nanoclusters similar to those in the hydrotreating catalysts. The supported nanoclusters are structurally and electronically similar to free MoS_2 and are found to interact rather weakly with the inert gold substrate, meaning that we study atomic-scale properties relevant for free Co–Mo–S-type nanoclusters. For further details concerning the synthesis and use of Au as a model substrate, we refer to Refs. [26,27]. The experiments in this paper were performed in an ultra-high-vacuum (UHV) chamber with a base pressure below 1×10^{-10} mbar. The chamber is equipped with standard equipment for surface preparation and analysis with Auger electron spectroscopy (AES). For metal deposition, we used a four-pocket e-beam evaporator (Oxford Applied Research EGCO4) capable of evaporating refractory metal at a finely controlled and reproducible rate. The high-resolution STM results were obtained by a home-built Aarhus-type STM [28].

To synthesize the mixed bimetallic sulfides corresponding to a Me–Mo–S phase, we took great care to optimize the synthesis conditions. Our previous detailed studies for Co–Mo–S and Ni–Mo–S [6,7] have shown that it is important to follow a sequence that involves first continuous deposition of Mo for 8 min followed by co-deposition for 2 min of Mo together with the dopant metal (Me = Mn, Fe, Co, Ni, or Cu) in a sulfiding atmosphere of 1×10^{-6} mbar of H_2S. This method suppressed phase separation into the separate monometallic sulfides and generally leads to the most uniform ensemble of clusters indicating that the equilibrium shape has been achieved. As a final step, the metal deposition is then terminated and the sample undergoes post-annealing at 673 K while maintaining the sulfiding atmosphere of 10^{-6} mbar of H_2S to crystallize the nanoclusters. Metal coverages were determined individually to be 10% of a monolayer (ML) for Mo and 4% ML of promoter metal (Me), corresponding to a large excess relative to the amount of dopant present in the mixed metal sulfide clusters. Syntheses with even higher coverages of the dopant metals did not change the morphology of the synthesized MoS_2-based nanoclusters as will be discussed later on.

2.2. Synthesis and activity of industrial-style hydrotreating catalysts

2.2.1. Catalyst preparation

Five unactivated, i.e., unsulfided, catalyst samples (Mo, FeMo, CoMo, NiMo, and CuMo) were made on the same active granular carbon support (multipoint BET surface area 900 m^2/g, average pore diameter 28 Å). Incipient wetness impregnation was used for all catalysts, but whereas most could be made by one-step impregnation, solubility did not allow this for CuMo. The concentrations of the impregnation liquids were chosen so as in all cases to give the same loading of metals on the carrier. Impregnation liquids were made by (sometimes heat-assisted) dissolution of $H_4[SiMo_{12}O_{40}]{\cdot}xH_2O$ in water, either alone (for the unpromoted catalyst) or together with iron(II) oxalate, cobalt(II) hydroxide or nickel-hydroxocarbonate. In the case of the FeMo catalyst, a small amount of H_2O_2 was added in order to aid dissolution of the iron compound. The impregnated samples were dried at 250 °C for 2 h. The CuMo catalyst was made by impregnating the Mo sample with Cu in the form of aqueous copper(II) acetate solution followed by drying at 250 °C for 2 h. For all MeMo catalysts, the atomic ratio Me:Mo = 1:3 was the target and analysis of the dried catalysts by ICP showed this to have been achieved: Mo catalyst 8.9 wt% Mo; FeMo catalyst 8.5 wt% Mo, 1.9 wt% Fe; CoMo catalyst 8.8 wt% Mo, 1.8 wt% Co; NiMo catalyst 9.0 wt% Mo, 1.9 wt% Ni. The CuMo catalyst was not analyzed in its final state as the Cu load is well defined from the concentration of the copper(II) acetate impregnation liquids and as the Mo load of the Mo catalyst from which it was made had already been measured.

2.2.2. Catalyst sulfidation and catalytic measurements

Catalytic tests were made in a tubular 7.5-mm-inner-diameter, high-pressure reactor loaded with a mixture of 0.30 g catalyst in

the form of 600–850 μm mesh granulates and glass microbeads. The feed was an *n*-heptane solution containing 3.0% dibenzothiophene, 0.5% indole, 1.0% naphthalene, 2.5% dimethyldisulfide, and 0.5% *n*-nonane. The latter substance was added to serve as internal GC standard. Upon entry into the hot reactor, the liquid feed evaporated and was mixed with a stream of H_2. The total pressure (reactants + *n*-heptane + H_2) at the reactor temperature of 350 °C was 50 atm corresponding to $p(H_2) = 38$ atm. Liquid feed to gaseous H_2 ratio was 0.5 ml/min:250 Nml/min. Under these conditions, all dimethyldisulfide in the feed quickly undergoes complete hydrodesulfurization to produce a background partial pressure of H_2S in the reactor. This partial pressure of H_2S ensures that catalysts remain fully sulfided during the catalytic tests. In order to ensure that catalysts are fully sulfided before catalytic tests, *in situ* sulfidation was made for 4 h at 350 °C by means of a 2.5% solution of dimethyldisulfide (DMDS) in *n*-heptane and with $p(H_2) = 42$ atm.

During the 24-h catalytic test of a catalyst sample, the composition of the exit gas from the reactor was continuously determined and quantified by GC–FID. The retention times of the various reactant and product species were known from previous GC–MS analyses using the same column (non-polar WCOT, Hewlett-Packard Ultra 2) as the GC–FID. Under the reaction conditions employed, the catalysts in question gives rise to the following reactions: dibenzothiophene (DBT) is desulfurized by two parallel routes yielding either biphenyl (BP) or cyclohexylbenzene (CHB) as products. Indole is denitrogenated to yield ethylbenzene and ethylcyclohexane as products. Naphthalene is hydrogenated to tetralene. The conversions determined were expressed as pseudo first-order rate constants for hydrodesulfurization (HDS), hydrodenitrogenation (HDN), and hydrogenation (HYD).

3. Results and discussion

3.1. Me–Mo–S morphology

The synthesis of Me–Mo–S is observed with STM to result in two distinctly different types of surface structures for the four different systems (see Fig. 1): (i) iron, cobalt, and nickel sulfide form as larger extended islands form at the Au(1 1 1) step edges (in the case of copper, metallic Cu islands form and only the rim of these islands is sulfided), and (ii) well-dispersed, flat-lying Fe–Mo–S, Co–Mo–S, Ni–Mo–S, and Cu–Mo–S nanoclusters dispersed on the terraces of the Au(1 1 1) substrate. The formation of large iron, cobalt, or nickel sulfide and of metallic copper islands is expected as the amounts of dopant atoms added during the synthesis exceeds the number of substitution sites available on the MoS_2 nanoclusters. All sulfide structures in Fig. 1a–d were identified in separate atom-resolved STM experiments involving sulfidation of *only* the Me-dopant [29]. As Fe, Co, Ni, and Cu sulfides possess negligible HDS reactivity [2], the discussion in this paper will exclusively concern the catalytically interesting crystalline Me–Mo–S nanoclusters nucleated on the Au(1 1 1) terraces (Fig. 1e–h). However, it is worth noting that the kinetics involved in the formation of these pure dopant sulfides is very complex [29] and is a crucially important factor in the activation of industrial, alumina-supported Co–Mo–S and Ni–Mo–S catalysts. Sometimes, special measures, such as the use of chelating agents, are taken to inhibit the formation of inactive Co and Ni sulfides [30].

The main indicator in the STM images for the formation of doped MoS_2 nanoclusters is a pronounced change in the equilibrium morphology of the Me–Mo–S nanoclusters relative to that of unpromoted MoS_2 nanoclusters. Atom-resolved STM images (Fig. 2) show that the interior part of all Me–Mo–S nanoclusters displays a hexagonal lattice with the 3.15 Å inter atomic S–S distance characteristic for a regular $MoS_2(0\,0\,0\,1)$ structure. The measured height of ~2.2 Å is indicative of a *single*-layer MoS_2 nanocluster [25]. However, whereas the non-doped MoS_2 nanoclusters synthesized under sulfiding conditions display a distinctly triangular shape [26], all the doped Me–Mo–S nanoclusters display truncated, i.e., hexagonal, shapes (Fig. 2). The shift in the morphology for Me–Mo–S relative to non-doped MoS_2 nanoclusters is invoked only by the presence of dopant atoms (all other synthesis parameters were the kept same), and the observed shift in morphology is directly attributed to the incorporation of dopant atoms into the MoS_2 structure, i.e., the formation of a Fe–Mo–S, Co–Mo–S, Ni–Mo–S, or Cu–Mo–S phase, respectively. Previous EXAFS and Mössbauer spectroscopy studies have found the existence of an Fe–Mo–S phase similar to the Co–Mo–S and Ni–Mo–S phases [31–34], whereas a Cu–Mo–S phase has never been detected and was mostly considered to be unfavorable due to the weak Cu–S bond [35]. The present STM measurements thus confirm the existence of the Fe–Mo–S phase and reveal that a Cu–Mo–S phase in fact does exist.

A detailed analysis of the morphology of the doped Me–Mo–S phases (Fig. 1) reveals that significant differences exist between Fe–Mo–S, Co–Mo–S, Ni–Mo–S, and Cu–Mo–S nanoclusters. The detailed equilibrium shape of the doped MoS_2 nanoclusters depends significantly on the type of Me atom. From the series of STM images of the Me–Mo–S nanoclusters displayed in Fig. 2b–f, it is observed that the degree of truncation decreases when the number of valence shell electrons of the dopant element is increased, with Fe–Mo–S nanoclusters having the most truncated shapes.

To quantify this distinct effect for the Me–Mo–S nanocluster shape, we treat the hexagonally truncated triangular Me–Mo–S nanoclusters as single-layer MoS_2 nanoclusters with the edges perturbed by incorporation of Me atoms as illustrated in Fig. 3 [36]. The shape of a free MoS_2 nanoparticle can be described in terms of a Wulff construction in which the relative edge free energies of the low-index $(\bar{1}010)$ S-edges and $(10\bar{1}0)$ Mo-edges (γ_S and γ_{Mo}, respectively), the two types of edges that terminate the particle, describe the equilibrium shape [27,37]. The very distinct triangular shape of non-doped MoS_2 nanoclusters (Fig. 2a) exposing only fully sulfided $(10\bar{1}0)$ Mo-edges reflects that the edge free energy of the S-edge exceeds that of the Mo-edge by more than a factor of two [26]. The hexagonal shape of the metal-doped nanoclusters, on the other hand, implies that two types of low-index edge terminations of the $MoS_2(0\,0\,0\,1)$ basal plane are present, i.e., both $(10\bar{1}0)$ Mo-edges and $(\bar{1}010)$ S-edges are exposed (see Fig. 3). In terms of edge free energies, this implies that the ratio of γ_S and γ_{Mo} for a given Me–Mo–S clusters is in the range 0.5–2. In other words, the S-edge becomes energetically stabilized relative to the Mo-edge by incorporation of Me atoms. In the experiments, we systematically investigated whether the detailed shape dependence on the type of Me-dopant atoms could be caused by a deficit of available dopant atoms during the syntheses. However, whereas the standard synthesis involved a total coverage of the dopant metal at ~4% ML, an increase to ~20% ML did not lead to a significant change in cluster shape. In fact, the general observation was that when the MoS_2 nanoclusters were saturated with dopant atoms, deposition of additional dopant atoms on the Au(1 1 1) surface only led to growth of larger dopant monometallic sulfide islands (e.g., Co_3S_4). This observation strongly suggests that the shape of the Me-doped Me–Mo–S nanoclusters reflects equilibrium structures and that different types of Me atoms indeed have different affinities for becoming incorporated into the MoS_2 nanoclusters.

The systematic decrease in degree of truncation as a function of the number of valence shell electrons of the Me-dopant atom directly reflects the change in the surface free energies gained by incorporation of the promoters. For each of the four different Me-

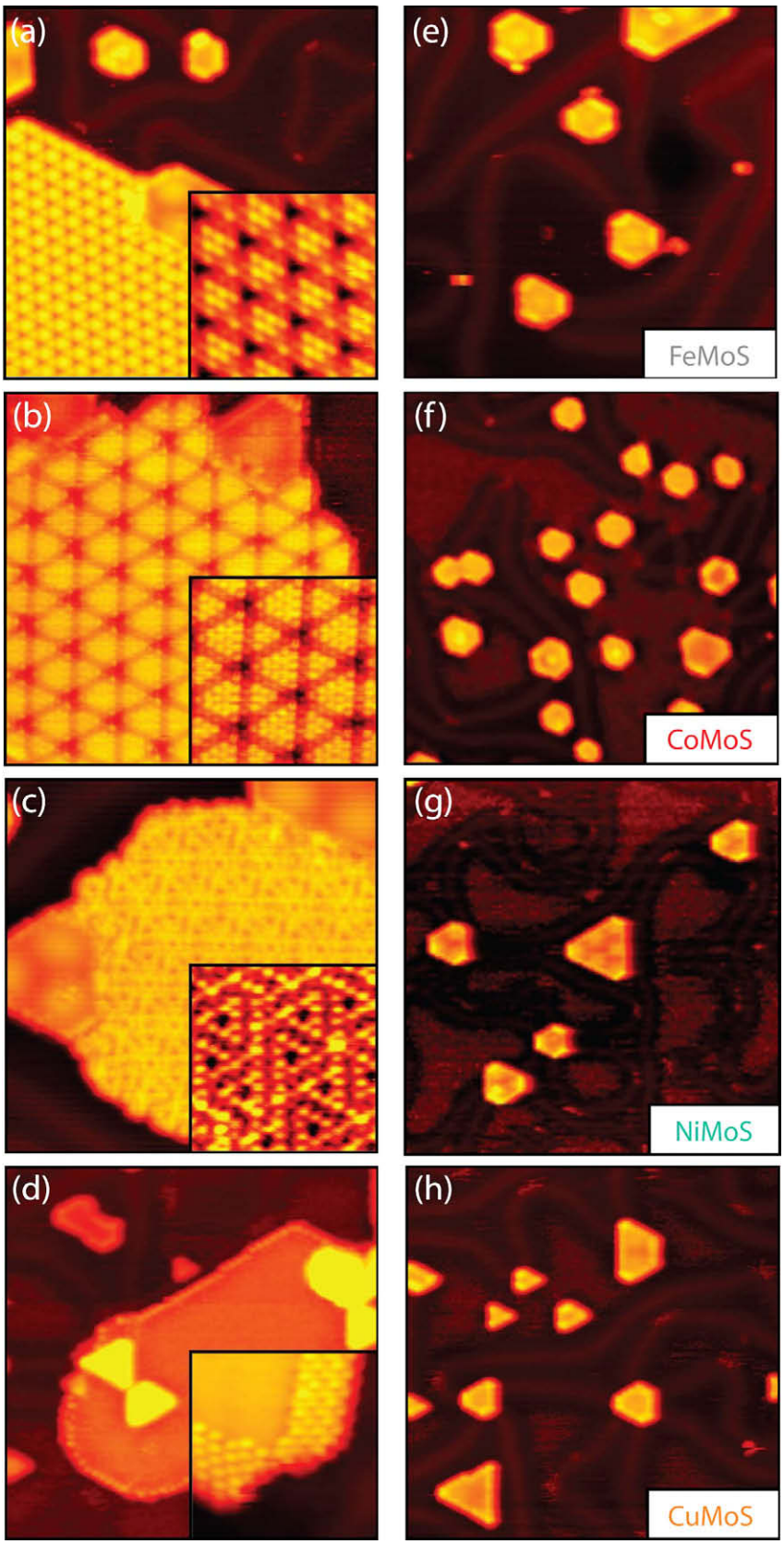

Fig. 1. (a)–(d) STM images of the pure Me sulfide structures: (a) iron sulfide (275 Å × 275 Å, inset 50 Å × 50 Å), (b) cobalt sulfide (150 Å × 150 Å, inset 60 Å × 60 Å), (c) nickel sulfide (175 Å × 175 Å, inset 50 Å × 50 Å), and (d) metallic Cu island with only the rim sulfided (275 Å × 275 Å, inset 55 Å × 55 Å). The insets show atom-resolved STM images of the structures. (e)–(h) STM images of the doped MoS_2 nanoclusters: (e) Fe–Mo–S nanoclusters (250 Å × 250 Å), (f) Co–Mo–S nanoclusters (400 Å × 400 Å), (g) Ni–Mo–S nanoclusters (500 Å × 500 Å), and (h) Cu–Mo–S nanoclusters (300 Å × 300 Å).

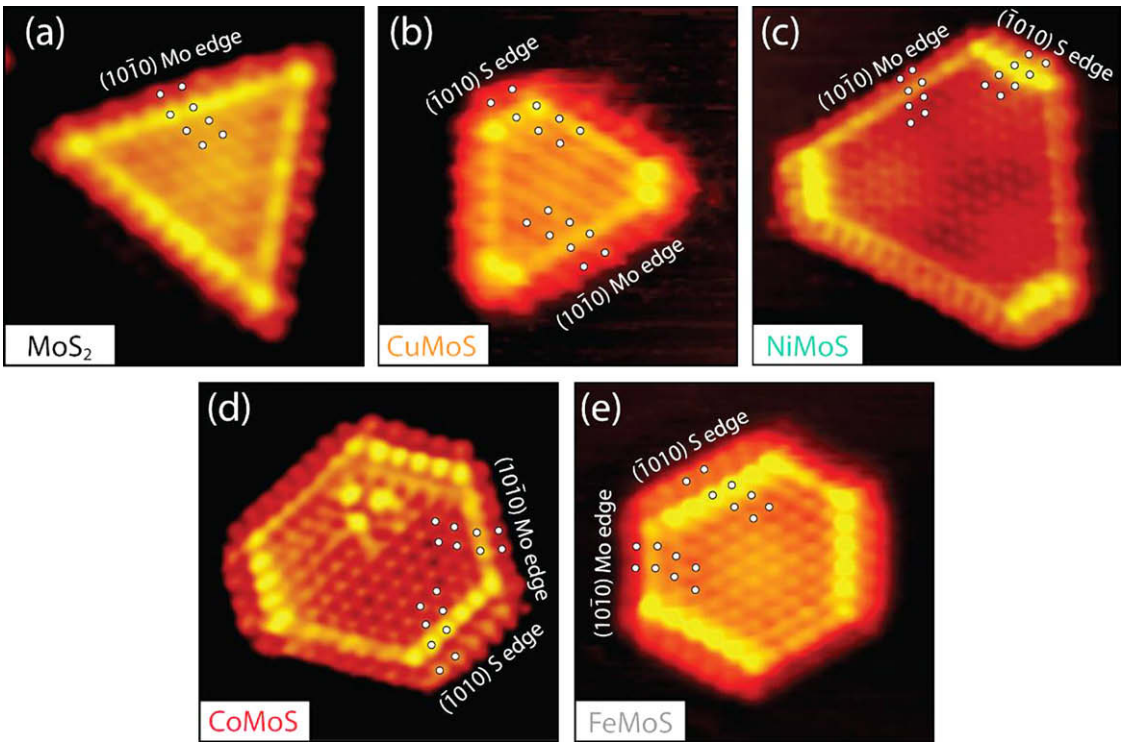

Fig. 2. Atom-resolved STM images of: (a) non-doped MoS_2 (50 Å × 50 Å, I_t = 1.290 nA, V_t = 5.2 mV), (b) Cu–Mo–S (50 Å × 50 Å, I_t = 0.660 nA, V_t = −3.4 mV), (c) Ni–Mo–S (67 Å × 65 Å, I_t = 0.500 nA, V_t = −600 mV), (d) Co–Mo–S (51 Å × 52 Å, I_t = 0.81 nA, V_t = 95.2 mV), and (e) Fe–Mo–S (50 Å × 50 Å, I_t = 0.790 nA, V_t = −132 mV) nanoclusters, respectively. The white dots illustrate the position of the protrusions.

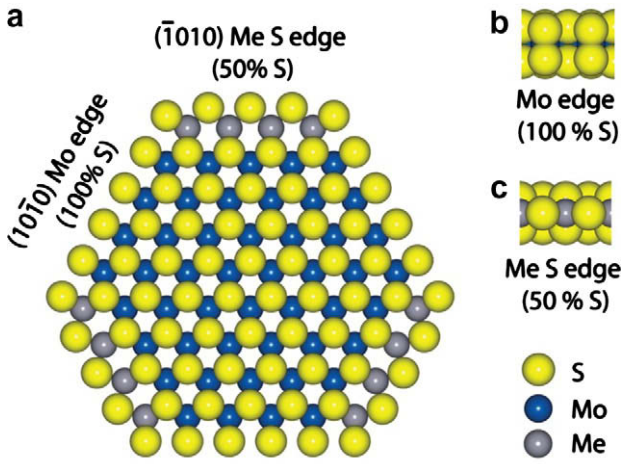

Fig. 3. (a) Ball model of a dopant atom-substituted MoS_2 nanocluster. (b) Side view of the (10$\bar{1}$0) Mo-edge. (c) Side view of the Me atom substituted ($\bar{1}$010) S-edge (Me = Fe, Co, Ni, or Cu).

doped MoS_2 nanoclusters, the effect can be geometrically quantified by the ratio (l_S/l_{tot}) of the total length of the ($\bar{1}$010) S-edges (l_S) to the total edge length (l_{tot}). Since a variation in nanocluster shape is always observed, the data are presented as distributions (Fig. 4a). The distributions of l_S/l_{tot} clearly reveal that the proportional length of the doped ($\bar{1}$010) S-edges decreases when the number of valence shell electrons of the dopant atom is increased, i.e., the energy gain associated with incorporation of Me atoms into the S-edge increases in the order Fe > Co > Ni > Cu. The mean values of the l_S/l_{tot} ratios are displayed in Fig. 4b together with the corresponding derived edge free energy ratios (γ_S/γ_{Mo}). Qualitatively, the Cu–Mo–S clusters thus appear almost triangular with only a very slight degree of truncation, whereas the Fe–Mo–S clusters exhibit a more pronounced hexagonal shape with an equivalent amount of doped S-edge and unpromoted Mo-edge edges. The catalytically superior Co–Mo–S and Ni–Mo–S clusters display intermediate degrees of truncation. Interestingly, we observe here that the preference to form promoted edges in Me–Mo–S nanoclusters correlates with the strength of the particular Me–S bond reported in Refs. [18,19,38], i.e., stronger Me–S bond leads to higher degree of truncation of Me–Mo–S and thus more Me-doped sites. Following the trend in Ref. [18], manganese-doped nanoclusters (Mn–Mo–S) should exhibit a significantly truncated shape. We attempted to synthesize such nanoclusters by the same synthesis procedure as used in the other cases. However, the synthesis produced well-separated manganese sulfide and unpromoted MoS_2 nanoclusters where only a small fraction of the clusters contained small amounts of Mn, presumably due to an extremely fast sulfidation of Mn.

3.2. Me–Mo–S edge structures

Atom-resolved STM images reveal that the edge structures of the Cu–Mo–S and Fe–Mo–S nanoclusters (Fig. 2b and e) appear quite similar to those of Co–Mo–S and Ni–Mo–S (Fig. 2c and d), which were previously analyzed in great detail in Refs. [6,7]. The Mo-edges of the hexagonally truncated Me–Mo–S nanoclusters are identified by a bright brim located adjacent to the outermost row of protrusions and a shift of half a lattice constant of the outermost protrusions relative to the sulfur lattice of the basal plane was revealed, as indicated by the superimposed dots. The Mo-edges on all Me–Mo–S nanoclusters are qualitatively and quantitatively identical to the edges of the non-doped MoS_2 nanoclusters (Fig. 2a) and are accordingly ascribed to fully sulfided (10$\bar{1}$0) Mo-edges [27]. We therefore conclude that Me-dopant atoms have no affinity to the (10$\bar{1}$0) Mo-edges and that these edges in Me–

a

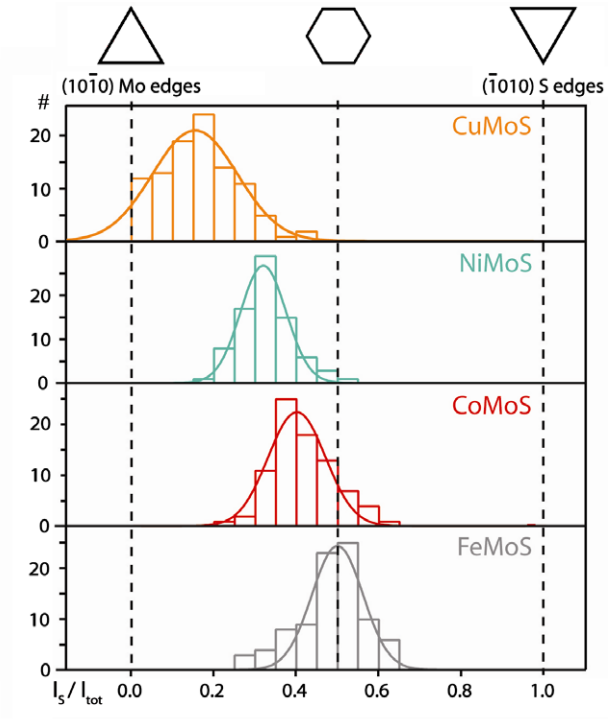

b

	CuMoS	NiMoS	CoMoS	FeMoS
I_S/I_{tot}	0.17±0.01	0.33±0.01	0.42±0.01	0.48±0.01
$\gamma_S/\gamma_{Mo} = \frac{2 - I_S/I_{tot}}{1 + I_S/I_{tot}}$	1.56±0.02	1.26±0.02	1.11±0.02	1.03±0.02

Fig. 4. (a) Distributions of the ratio of the length of the S-edges to the total edge length (l_S/l_{tot}) for Cu–Mo–S, Ni–Mo–S, Co–Mo–S, and Fe–Mo–S, respectively. (b) Table of the mean values of the l_S/l_{tot} ratio and the corresponding edge free energy ratios: γ_S/γ_{Mo}.

Mo–S catalysts consequently should have the same intrinsic catalytic properties as unpromoted MoS_2 nanoclusters terminated by Mo-edges.

The other edge type in the Cu–Mo–S and Fe–Mo–S nanoclusters is according to the symmetry of the MoS_2 crystal structure assigned to ($\bar{1}$010) S-edges. Previous STM studies of Co–Mo–S and Ni–Mo–S have shown that the ($\bar{1}$010) S-edges are terminated by bridging S atoms (monomers = "50% S") with tetrahedrally sulfur-coordinated Ni or Co atoms at the edges (Fig. 3a and c) [6,7]. These edges are characterized in STM images by an intense bright brim located behind the outermost row of protrusions that are located *in-registry* with the basal plane atoms, as indicated with the dots in Fig. 2c and d. From the strong resemblance of Cu–Mo–S (Fig. 2b) and Fe–Mo–S (Fig. 2e) with Co–Mo–S and Ni–Mo–S and the fact that the single 3.15 Å periodicity is retained for the edges, we conclude that the ($\bar{1}$010) S-edges of the Cu–Mo–S and Fe–Mo–S phase are also fully (100% Me) substituted with Cu or Fe at the original Mo sites. The sulfur coverages for the Cu–Mo–S and Fe–Mo–S S-edges are not explicitly determined from the STM contrast since electronic effects may influence the height of the S atoms. The similar level of contrast of all protrusions and their in-registry positions are in principle compatible with both a 50% and a 100% S coverage on the S-edge [7,10,39]. In the previous studies [7], it was confirmed by a comparison of experimentally recorded STM images and simulated STM images based on the simple Tersoff Hamman model that such an STM appearance reflects a 50% sulfur coverage for Co–Mo–S and Ni–Mo–S, and given the very close similarity of the outermost protrusion on the S-edges of Fe–Mo–S and Cu–Mo–S, we tentatively assign a similar S coverage of 50% here. We thus suggest that Cu and Fe then adopt a tetrahedral coordination by four S atoms, which is not unexpected for these metals.

Overall, the edge structures of Fe–Mo–S and Cu–Mo–S nanoclusters appear similar to those of the Co–Mo–S and Ni–Mo–S nanoclusters, and the driving force for the observed morphological shift from a triangular shape for non-doped MoS_2 nanoclusters toward a hexagonally truncated shape for the doped MoS_2 nanoclusters is attributed to the tendency for the dopant atoms to be located *only* at the ($\bar{1}$010) S-edges independent of the nature of the dopant atom. The degree of truncation of the nanoclusters depends uniquely on the type of dopant atom, and we expect this observation to hold also for the industrial catalysts since results from DFT calculations show that the more reducing environment for the hydrotreating process disfavors dopant atoms at the (10$\bar{1}$0) Mo-edges when compared to the sulfiding conditions of the synthesis and STM imaging conditions of the model catalyst [11].

We also note that the Ni–Mo–S nanoclusters have been shown to exhibit a size-dependent morphology where normal NiMoS clusters (type A) display the morphology described above, whereas even smaller clusters (type B NiMoS) are further truncated by substitution of Mo at the corner site between the S- and Mo-edges [7]. However, we do not observe a similar size-dependent morphology for any of the other dopants and only substitution of the Me at the S-edge was therefore considered for the comparative analysis presented here.

3.3. Structure and activity correlations for Me–Mo–S nanoclusters

To link the STM morphology studies of the Me–Mo–S model catalysts to the industrial catalyst and establish to which extent a fundamental correlation exists between the atomic-scale structure and the observed catalytic activities and selectivities, we have synthesized a comparable set of Me–Mo–S catalysts supported on a high-surface carbon and measured their activities. The choice of carbon as support was motivated by the intention to characterize catalyst particles with a similar weak bonding to the substrate as the model system used for STM. Previous High-Angle Annular Dark-field Scanning Transmission Electron Microscopy (HAADF-STEM) has determined that the truncated single-layer Co–Mo–S and Ni–Mo–S morphologies for graphite-supported catalysts are consistent with those observed in the STM experiments [40]. The industrial high-surface-area catalysts were prepared with the identical metal loadings and atomic ratio Me:Mo = 1:3 as described in Section 2, to enable the best possible quantitative cross-correlation of the activities and selectivity for each Me-dopant.

Hydrodesulfurization (HDS) activity was measured as the conversion of dibenzothiophene (DBT). According to previous studies, the HDS reaction can proceed through two main pathways, the direct desulfurization (DDS) pathway and the hydrogenation (HYD) pathway, with a relative importance that depends on the type of promoter [2,41–43]. For the DDS pathway, sulfur is directly extruded and the main product is biphenyl (BP) whereas during the hydrogenation pathway, one of double bonds in the aromatic structure is saturated prior to C–S cleavage and cyclohexylbenzene (CHB) is formed as the main product. We have measured the rate constants for the formation of both products: k(BP) (reflecting the selectivity for the DDS route for HDS) and k(CHB) (reflecting the selectivity for the HYD route for HDS). In addition, the activity k(HDN), for hydrodenitrogenation of indole, and activity k(HYD),

for hydrogenation of naphthalene, were measured (see Section 2 for details).

Fig. 5a shows a table of the five measured rate constants used to express the catalytic activities of the five different samples (unpromoted MoS_2 and four Me–Mo–S catalysts). The corresponding plot of the activities as a function of the number of valence shell electrons of the dopant metal in Fig. 5b demonstrates a typical "vulcano" shape and is qualitatively similar to those previously reported [16,44,45]. Interestingly, the plot reveals an almost uniform variation in all activity parameters as a function of dopant metal. The Ni–Mo–S catalyst displays the highest catalytic activity for all five reactions followed by Co–Mo–S, whereas the Fe–Mo–S and Cu–Mo–S catalysts on either side of the peak display activities similar to unpromoted MoS_2. The low activity of Fe–Mo–S for all five catalytic reactions studied is striking, since Fe–Mo–S nanoclusters expose the largest number of doped S-edge sites of the four Me–Mo–S structures. Clearly, the non-promoting role of Fe must be related to an unfavorable intrinsic catalytic property of the Fe–Mo–S S-edge [17]. We can quantify the intrinsic catalytic activity in a model where the overall activity, k, is a linear combination of contributions from the unpromoted Mo-edge k_{Mo} and the promoted S-edge, k_{Me}, weighted by the ratio of the edge lengths defined by the parameter $\alpha = l_S/l_{tot}$:

$$k = (1-\alpha)k_{Mo} + \alpha k_{Me} \quad (1)$$

Using this model, we can decouple the intrinsic activity, k_{Me}, of the promoted edges from the total activity. Fig. 6a shows a table of the intrinsic HDS, HDN, and HYD rate constants for the doped $(\bar{1}010)$ S-edges, k_{Me}, calculated from Eq. (1) using the l_S/l_{tot} values in Fig. 4b and the k_{Mo} values in Fig. 5a. The corresponding plot of the k_{Me} rate constants versus dopant in Fig. 6b displays a steeper "volcano" shape than the plot in Fig. 5b. Whereas the k_{Ni} values are about

a

	MoS_2	FeMoS	CoMoS	NiMoS	CuMoS
k(HDS) [h^{-1}]	8	6	72	167	3
k(BP) [h^{-1}]	4	4	45	101	2
k(CHB) [h^{-1}]	3	3	27	65	1
k(HYD) [h^{-1}]	11	11	46	101	4
k(HDN) [h^{-1}]	9	9	26	74	4

b

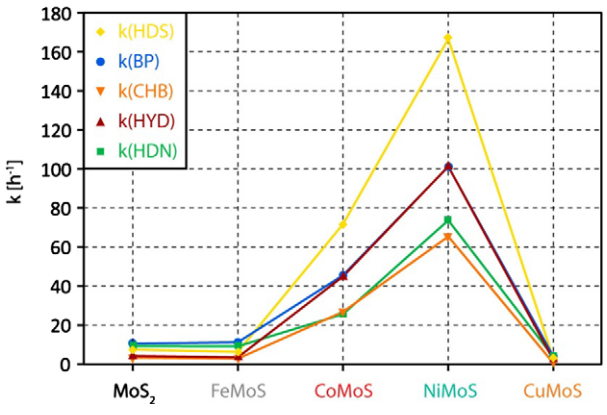

Fig. 5. (a) Table of hydrodesulfurization (HDS), hydrodenitrogenation (HDN), and hydrogenation (HYD) rate constants measured for industrial-style carbon-supported catalysts. The overall HDS rate constant, k(HDS), is the sum of k(BP) and k(CHB), which express the HDS activities with respect to the direct desulfurization pathway (DDS) and the hydrogenation pathway, respectively. (b) Plot of the rate constants from the table in (a).

a

	Fe	Co	Ni	Cu
k_{Me}(HDS) [h^{-1}]	5	161	490	-20
k_{Me}(BP) [h^{-1}]	3	101	298	-7
k_{Me}(CHB) [h^{-1}]	2	59	192	-13
k_{Me}(HYD) [h^{-1}]	12	94	285	-28
k_{Me}(HDN) [h^{-1}]	9	48	205	-24

b

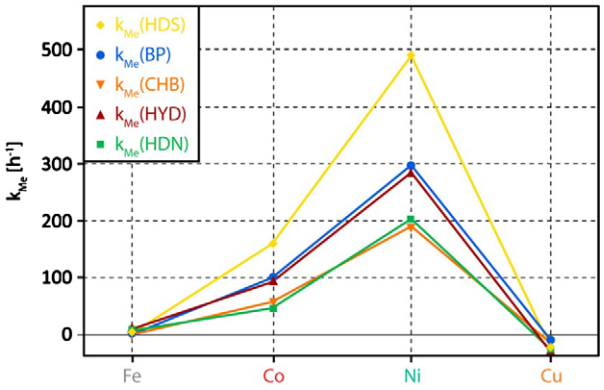

Fig. 6. (a) Table of the intrinsic HDS, HDN, and HYD rate constants for doped S-edges, k_{Me}. The values have been extracted from the data in Figs. 4 and 5 and Eq. (1). The negative values for k_{Cu} are hypothetical reflecting that Cu lowers the activity relative to unpromoted MoS_2. (b) Detailed plot of the rate constants from the table in (a).

three times larger than the k_{Co} values, the overall activity of Ni–Mo–S nanoclusters is only about two times higher than Co–Mo–S nanoclusters, due to the fact that Co–Mo–S exposes more promoted sites than Ni–Mo–S. For Cu–Mo–S, the slightly negative k_{Cu} have no direct physical significance but reflect that in the simple model of Eq. (1), the Cu-doped S-edges give a negative contribution to the overall rate constants, i.e., the Cu substitution on the S-edges reduces the catalytic activity. These results emphasize the importance that the geometric factor is taken into account when describing the promoting effect in absolute numbers.

The STM results in this experimental study explicitly show that the preferred substitution site of Fe, Ni, Co, and Cu atoms is at the Me–Mo–S $(\bar{1}010)$ S-edges, and we can conclude that the activity variations are mainly related to the intrinsic catalytic properties of these edges. Previous studies have, in the context of the Sabatier principle [46], emphasized the direct Me–S bond energy as the primary parameter describing the activity [18–20]. Binding energies of S on the Ni–Mo–S and Co–Mo–S $(\bar{1}010)$ S-edges are already rather well characterized from previous DFT studies [7,9,10,47]. Moses et al. [24] recently reported a very high formation energy of S-vacancies on the "50% S" Co–Mo–S S-edge (Fig. 2c) that seems to disagree with finding that Co acts as a good promoter, but the same study also showed that the built-in undercoordination of the "50% S" Co–Mo–S S-edge leads to a favorable bonding of S-bearing hydrocarbons *without* the need to form S-vacancies. Following the trends for the S–Me bonding strength reported in the previous studies [17], we tentatively suggest that the Ni–Mo–S S-edge with 50% S coverage has a similar favorable inherent adsorption strength whereas the Fe–Mo–S S-edge with "50% S" would bind the S-bearing molecules too strongly or even be "100% S" under conditions corresponding to industrial HDS operation. For Cu–Mo–S on the other hand, the sulfur adsorption is presumably too weak and prevents the adsorption of S-bearing molecules [9], which explains the slight anti-promoting effect of Cu ($k_{Cu} < 0$) for

all reactions in Fig. 6. A second important factor, which is examined to a much lesser extent for Me–Mo–S nanoclusters, is the hydrogenation properties of the Me–Mo–S S-edges, which have not been considered in detail in the previous theoretical studies [10,48–50]. In this case, it is important to obtain a detailed information of the adsorption strength of H, and the barrier for dissociative adsorption of hydrogen gas (H_2) on the $(\bar{1}010)$ Me–Mo–S S-edges is necessary to shed more light on the activity of the Me–Mo–S. We speculate that variations of the bonding of H on the Me–Mo–S S-edge could be an overriding factor determining both the DDS reaction and HYD reactions, since a too weak/strong bonding of H (and thus a too low/high H coverage on the Me–Mo–S S-edges) would significantly impede the key reaction steps involving transfer of H from the cluster edges. Indeed, for the "50% S" Me–Mo–S S-edge, the expected trend is that H adsorption strength decreases with increasing Me–S bonding energy [50], which would then explain the rather low overall activity of Fe–Mo–S. Future theoretical studies and/or H–D exchange studies for Fe–Mo–S are needed to shed more light on this issue.

4. Conclusions

Using STM and activity measurements, we have investigated the variations in the atomic-scale structure and morphology of Me-doped MoS_2 nanoclusters (Me = Fe, Co, Ni, and Cu) in order to establish a fundamental correlation between the atomic-scale structure and the activity of Me–Mo–S in hydrotreating catalysis. The results reveal that all four types of dopant metals facilitate the formation of mixed "Me–Mo–S"-type structures shaped as single-layer, hexagonally truncated triangular MoS_2-like nanoclusters. This morphology is controlled by the tendency of the dopant atoms to become incorporated at only the $(\bar{1}010)$ S-edges. However, the degree of truncation is found to depend on the type of dopant atoms in a systematic way, and we find a direct correlation between the proportional length of the Me-stabilized edges and the bonding strength of Me to sulfur. In terms of catalytic performance, we conclude that the overall variation in the so-called volcano plot of catalytic activity versus the Me-dopant is mainly controlled by the intrinsic catalytic properties of the promoted S-edges, modulated by a geometric effect reflecting the length of the promoted edges. The importance of the intrinsic effect is clearly revealed in the case of Fe–Mo–S nanoclusters, which expose the largest number of doped S-edge sites of the four Me–Mo–S structures but have an activity comparable with non-doped MoS_2. The observed absence of promotion by Fe is explained as an intrinsic effect of the Fe–Mo–S S-edge, which we tentatively attribute to a too strong Me–S interaction and a too weak H adsorption strength. The Co–Mo–S and Ni–Mo–S nanoclusters seem to offer an optimum of both the geometric and intrinsic effect, i.e., an optimum number of active promoted sites and a good combination of Me–S bonding and H adsorption strength. Future attempts to improve catalytic activity should therefore mainly focus on the geometric factor, i.e., by optimizing the S-edges of Co–Mo–S and Ni–Mo–S investigated in this study. Such a scheme may, for example, involve controlled synthesis of Co–Mo–S-type structures on more strongly interacting metal oxide substrates such as TiO_2 [51] or Al_2O_3, thereby forcing the growth of "perturbed" Co–Mo–S shapes reflecting longer S-edges relative to the equilibrium situation in this study.

Acknowledgments

The iNANO group gratefully acknowledges financial support from The Danish Research Councils and The Strategic Research Council (*NABIIT project "Development of new metal-oxide and -sulphide catalysts*"). We furthermore acknowledges financial support from the Lundbeck Foundation, the Villum Kann Rasmussen Foundation and the European Research Council through an ERC Starting Independent Researcher Grant #239834 (J.V.L.) and an Advanced Research Grant (F.B.E.).

References

[1] R. Prins, in: G. Ertl, H. Knözinger, F. Schüth, J. Weitkamp (Eds.), Handbook of Heterogeneous Catalysis, Wiley-VHC, Wienheim, p. 2695.
[2] H. Topsøe, B.S. Clausen, F.E. Massoth, Hydrotreating Catalysis Science and Technology, Springer Verlag, Berlin, 1996.
[3] T.A. Pecoraro, R.R. Chianelli, J. Catal. 67 (1981) 430–445.
[4] C. Wivel, R. Candia, B.S. Clausen, S. Mørup, H. Topsøe, J. Catal. 68 (1981) 453–463.
[5] N.-Y. Topsøe, H. Topsøe, J. Catal. 84 (1983) 386–401.
[6] J.V. Lauritsen, S. Helveg, E. Lægsgaard, I. Stensgaard, B.S. Clausen, H. Topsøe, F. Besenbacher, J. Catal. 197 (2001) 1–5.
[7] J.V. Lauritsen, J. Kibsgaard, G.H. Olesen, P.G. Moses, B. Hinnemann, S. Helveg, J.K. Nørskov, B.S. Clausen, H. Topsøe, E. Lægsgaard, F. Besenbacher, J. Catal. 249 (2007) 220–233.
[8] L.S. Byskov, B. Hammer, J.K. Nørskov, B.S. Clausen, H. Topsøe, Catal. Lett. 47 (1997) 177–182.
[9] P. Raybaud, J. Hafner, G. Kresse, S. Kasztelan, H. Toulhoat, J. Catal. 190 (2000) 128–143.
[10] H. Schweiger, P. Raybaud, H. Toulhoat, J. Catal. 212 (2002) 33–38.
[11] E. Krebs, B. Silvi, P. Raybaud, Catal. Today 130 (2008) 160–169.
[12] J.F. Paul, S. Cristol, E. Payen, Catal. Today 130 (2008) 139–148.
[13] H. Topsøe, B.S. Clausen, R. Candia, C. Wivel, S. Mørup, Bull. Soc. Chim. Belg. 90 (1981) 1189–1214.
[14] W.L.T.M. Ramselaar, M.W.J. Craje, E. Gerkema, V.H.J. de Beer, A.M. van der Kraan, Appl. Catal. 54 (1989) 217–239.
[15] H. Topsøe, R. Candia, N.-Y. Topsøe, B.S. Clausen, Bull. Soc. Chim. Belg. 93 (1984) 783–806.
[16] S. Harris, R.R. Chianelli, J. Catal. 98 (1986) 17–31.
[17] L.S. Byskov, J.K. Nørskov, B.S. Clausen, H. Topsøe, J. Catal. 187 (1999) 109–122.
[18] J.K. Nørskov, B.S. Clausen, H. Topsøe, Catal. Lett. 13 (1992) 1–8.
[19] H. Toulhoat, P. Raybaud, S. Kasztelan, G. Kresse, J. Hafner, Catal. Today 50 (1999) 629–636.
[20] R.R. Chianelli, G. Berhault, P. Raybaud, S. Kasztelan, J. Hafner, H. Toulhoat, Appl. Catal. A 227 (2002) 83–96.
[21] J.V. Lauritsen, M. Nyberg, R.T. Vang, M.V. Bollinger, B.S. Clausen, H. Topsøe, K.W. Jacobsen, F. Besenbacher, E. Lægsgaard, J.K. Nørskov, F. Besenbacher, Nanotechnology 14 (2003) 385–389.
[22] J.V. Lauritsen, M. Nyberg, J.K. Nørskov, B.S. Clausen, H. Topsøe, E. Lægsgaard, F. Besenbacher, J. Catal. 224 (2004) 94–106.
[23] P.G. Moses, B. Hinnemann, H. Topsøe, J.K. Nørskov, J. Catal. 260 (2008) 202–203.
[24] P.G. Moses, B. Hinnemann, H. Topsøe, J.K. Nørskov, J. Catal. 268 (2009) 201–208.
[25] J.V. Lauritsen, F. Besenbacher, Adv. Catal. 50 (2006) 97–143.
[26] S. Helveg, J.V. Lauritsen, E. Lægsgaard, I. Stensgaard, J.K. Nørskov, B.S. Clausen, H. Topsøe, F. Besenbacher, Phys. Rev. Lett. 84 (2000) 951–954.
[27] J.V. Lauritsen, M.V. Bollinger, E. Lægsgaard, K.W. Jacobsen, J.K. Nørskov, B.S. Clausen, H. Topsøe, F. Besenbacher, J. Catal. 221 (2004) 510–522.
[28] E. Lægsgaard, F. Besenbacher, K. Mortensen, I. Stensgaard, J. Microsc. 152 (1988) 663–669.
[29] J. Kibsgaard, K. Morgenstern, E. Lægsgaard, J.V. Lauritsen, F. Besenbacher, Phys. Rev. Lett. 100 (2008).
[30] L. Medici, R. Prins, J. Catal. 163 (1996) 38–49.
[31] H. Topsøe, R. Candia, N.Y. Topsøe, B.S. Clausen, Bull. Soc. Chim. Belg. 93 (1984) 783–806.
[32] W.L.T.M. Ramselaar, M.W.J. Craje, E. Gerkema, V.H.J. de Beer, A.M. van der Kraan, Bull. Soc. Chim. Belg. 96 (1987) 931–939.
[33] M.W.J. Craje, R.H. Hadders, W.L.T.M. Ramselaar, E. Gerkema, V.H.J. de Beer, A.M. van der Kraan, Hyperfine Interact. 57 (1990) 1801–1808.
[34] J.A. Moulijn, J. van Doorn, A.D. van Langeveld, P.J. Mangnus, S. Tajik, V.H.J. de Beer, N. Barthe-Zahir, S.M.A.M. Bouwens, J.N.M. van Gestel, E.M. van Oers, A.M. van der Kraan, M.W.J. Craje, W.L.T.M. Ramselaar, Int. J. Energy Res. 18 (1994) 127–143.
[35] G.U. Kulkarni, C.N.R. Rao, Catal. Lett. 9 (1991) 427–440.
[36] H. Toulhoat, S. Kasztelan, in: M.J. Phillips, M. Ternan (Eds.), Proceedings of the 9th International Congress on Catalysis, Calgary, Chemical Institute of Canada, Ottawa, 1988, pp. 152–159.
[37] H. Schweiger, P. Raybaud, G. Kresse, H. Toulhoat, J. Catal. 207 (2002) 76–87.
[38] H. Toulhoat, P. Raybaud, J. Catal. 216 (2003) 63–72.
[39] M.V. Bollinger, K.W. Jacobsen, J.K. Nørskov, Phys. Rev. B 67 (2003) 085410.
[40] M. Brorson, A. Carlsson, H. Topsøe, Catal. Today 123 (2007) 31–36.
[41] X. Li, A.J. Wang, M. Egorova, R. Prins, J. Catal. 250 (2007) 283–293.
[42] F. Bataille, J.-L. Lemberton, P. Michaud, G. Pérot, M. Vrinat, M. Lemaire, E. Schulz, M. Breysse, S. Kasztelan, J. Catal. 191 (2000) 409–422.
[43] M. Egorova, R. Prins, J. Catal. 225 (2004) 417–427.

[44] C. Thomazeau, C. Geantet, A. Lacroix, A. Danot, V. Harle, P. Raybaud, Appl. Catal. A 322 (2007) 92–97.
[45] A. Wambeke, H. Toulhoat, J.P. Boutrois, J. Grimblot, J.P. Bonnelle, in: B. Delmon, P. Grange, P.A. Jacobs, G. Poncelet (Eds.), Preparation of Catalysts IV, Elsevier, Amsterdam, pp. 581–589.
[46] P. Sabatier, Ber. Dtsch. Chem. Ges. 44 (1911) 1984.
[47] M.Y. Sun, A.E. Nelson, J. Adjaye, J. Catal. 226 (2004) 32–40.
[48] A. Travert, H. Nakamura, R.A. van Santen, S. Cristol, J.F. Paul, E. Payen, J. Am. Chem. Soc. 124 (2002) 7084–7095.
[49] M.Y. Sun, A.E. Nelson, J. Adjaye, Catal. Today 105 (2005) 36–43.
[50] M.Y. Sun, A.E. Nelson, J. Adjaye, J. Catal. 233 (2005) 411–421.
[51] J. Kibsgaard, B.S. Clausen, H. Topsøe, E. Lægsgaard, J.V. Lauritsen, F. Besenbacher, J. Catal. 263 (2009) 98–103.